Particle Transport Barriers Dependence on the Magnetic Configuration

Gabriel C. Grime[1], Marisa Roberto[2], Ricardo L. Viana[1,3], Yves Elskens[4], Iberê L. Caldas[1]

[1]*Institute of Physics - São Paulo University, São Paulo, Brazil*

[2]*Physics Department - Aeronautical Institute of Technology, São José dos Campos, Brazil*

[3]*Physics Department - Federal University of Paraná, Curitiba, Brazil*

[4]*Aix-Marseille Université, CNRS, UMR 7345 PIIM, F-13397 Marseille, France*

The control of radial particle transport in tokamak plasmas is a necessary condition for obtaining good confinement [1]. Such a goal can be achieved by creating internal transport barriers (ITBs): regions of reduced radial (cross field) particle transport in the plasma column [2]. ITBs have been produced in JET by the application of strong supplementary heating during the current rise phase of the plasma discharge [3]. The most widely studied type of ITB is the so-called edge transport barrier (ETB), related to steep pressure gradients at the plasma edge [4]. Recently, a second type of ITB has been investigated, the shearless transport barriers (STBs), which appears in tokamak plasmas with reversed shear profiles [5]. These profiles can be obtained by modifying the safety factor profile, and by applying radial electric fields in a specific way [6]. For example, reversed shear profiles of $q(r)$ have one or more extrema, at which shearless toroidal magnetic surfaces are formed [7]. Shearless surfaces represent ITBs in the sense that cross-field transport is reduced therein [4].

One of the characteristic features of anomalous cross-field transport in tokamak plasmas is the presence of electrostatic drift wave instabilities arising from density gradients [1]. A mathematical model for describing the test particle motion in drift waves has been proposed by Horton *et al.* [6]. This model consider a test particle subject to a combined equilibrium magnetic field $\mathbf{B}$ and an electric field $\mathbf{E}$ related to the electrostatic waves. Under these assumptions, the guiding-center motion has two components: (a) a passive advection along the magnetic field lines, with velocity $v_{\|}$ and (b) an $\mathbf{E}\times\mathbf{B}$ drift velocity, such that the guiding-center equation of motion is

$$\frac{d\mathbf{x}}{dt} = v_{\|}\frac{\mathbf{B}}{B} + \frac{\mathbf{E}\times\mathbf{B}}{B^2} \tag{1}$$

The tokamak equilibrium magnetic field has components B_φ and B_θ, the toroidal and poloidal magnetic field components, respectively. In the large aspect ratio approximation ($\varepsilon = a/R \ll 1$) $B \approx B_\varphi \gg B_\theta$. The safety factor of the magnetic surfaces is given by $q(r) = rB_\varphi/RB_\theta$. The electric field is the sum of an equilibrium radial electric component $\overline{\mathbf{E}_r}$ and a fluctuating part $\tilde{\mathbf{E}} = -\nabla\tilde{\phi}$ representing the electrostatic instabilities in tokamak edge [6]. The latter is modeled

by a Fourier expansion in the form [8]

$$\tilde{\phi}(\mathbf{x},t) = \sum_n \phi_n \cos\left(M\theta - L\varphi - n\omega_0 t + \alpha_n\right) \tag{2}$$

where the coefficients M and L are the dominant Fourier modes, with harmonics of the lowest frequency ω_0. Writing Eq. (1) in components, and considering action angle variables, $I = (r/a)^2$ and $\psi = M\theta - L\varphi$, we obtain the set of equations [6]:

$$\frac{dI}{dt} = 2M\sum_n \phi_n \sin(\psi - n\omega_o t), \tag{3a}$$

$$\frac{d\psi}{dt} = \varepsilon\frac{v_\parallel(I)}{q(I)}\left[M - Lq(I)\right] - \frac{M\overline{E_r}(I)}{\sqrt{I}}. \tag{3b}$$

Numerically integrating equations (3), we obtain stroboscopic Poincaré maps by plotting the trajectories in instants $t_j = j(2\pi/\omega_0)$. In order to numerically solve the equations (3) we use parameters of the TCABR tokamak, operating at the Physics Institute of São Paulo University (Brazil), which has $B_\varphi = 1.1\ T$ and aspect ratio $\varepsilon \approx 0.3$. Since we are interested chiefly in non-monotonic radial profiles, this model possesses transport barriers corresponding to shearless invariant curves in the phase space, defined by an extreme point in rotation number profile [7]. To every regular (nonchaotic) orbit we can associate a rotation number Ω given by the mean rotation angle in the Poincaré section. Given an initial condition (I_0, ψ_0), the rotation number of this orbit is given by:

$$\Omega = \lim_{n\to\infty} \sum_{i=0}^{n-1} \frac{(\psi_{i+1} - \psi_i)}{n}, \tag{4}$$

where ψ_i is the angle of i-th intersection in the Poincaré map.

Reversed shear profiles have been known to improve plasma confinement. In order to generate negative shear regions, it is necessary that the safety factor radial profile be non-monotonic. MHD-based models of a cylindrical plasma column suggest the following profile of the safety factor:

$$q(r) = q_a\frac{r^2}{a^2}\left[1 - \left(1 + \mu'\frac{r^2}{a^2}\right)\left(1 - \frac{r^2}{a^2}\right)^{\nu+1}\right]^{-1},\ \mu' = \mu\frac{\nu+1}{\mu+\nu+2} \tag{5}$$

where q_a is the safety factor at plasma edge. We fixed the parameters $\nu = 0.8$ and $q_0 = 3.75$, making the remaining parameter μ a function of q_a, which we choose as our control parameter. The $q(r)$ profile is plotted on Figure 1(a) for some values of the control parameter. The equilibrium electric field was chosen to be non-monotonic according $\overline{E_r}(r) = 3\alpha r^2 + 2\beta r + \gamma$, where $\alpha = -1.14$, $\beta = 2.529$, and $\gamma = -2.639$ are parameter values after a normalization. A normal-

ized parallel velocity profile to be used in this work, and consistent with TCABR observations, is given by $v_{\|}(I) = -3.15 + 5.58\tanh(14.1I + -9.26)$, once we apply the normalization factor $v_0 = E_0/B_0$. We assume the spatial dominant mode to have $M/L = 16/4$, which are typical

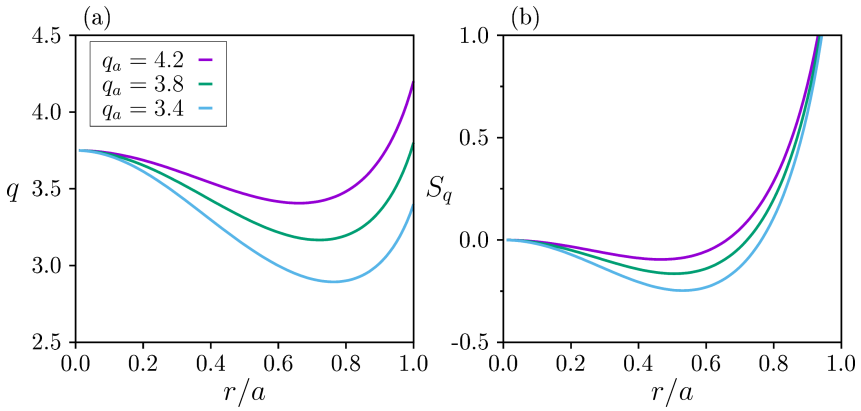

Figure 1: (a) Non-monotonic safety factor profile for some values of parameter q_a and magnetic shear profile (b).

numbers in the wave spectrum at the tokamak plasma edge [6]. The temporal modes considered are $n = 2,3,4$, based on the fluctuating spectrum of TCABR [8], with normalized amplitudes $(\phi_2, \phi_3, \phi_4) = (11.74, 2.077, 0.2443) \times 10^{-3}$. The fundamental frequency of the temporal modes is around 10 kHz, which implies in a normalized angular frequency $\omega_0 = 5.224$ [8]. Assuming that the rest of profiles and parameters are fixed, the safety factor will be chosen to be the tunable parameter which determines the dynamical behavior of the system.

The variation of the safety factor profile changes the behavior of shearless transport barrier. Figure 2 displays examples of Poincaré sections, in action-angle variables, for some values of control parameter q_a. In Figure 2(a), obtained for $q_a = 4.20$, we observe two large (twin) islands and a chaotic region around them. Between these twin islands there is a shearless curve, located at the action value corresponding to an extremum of the rotation number profile [Fig. 3(a)]. The chaotic region around the inner islands grows as the parameter q_a decreases and eventually causes the breakup of the shearless curve, depicted in [Fig. 2(b)] for $q_a = 3.44$. Noteworthy, if the value of q_a is further decreased, the shearless curve between the two twin islands reappears, as in [Fig. 2(c)] for $q_a = 3.40$, since the corresponding rotation number profile has an extremum for this parameter value [Fig. 3(b)].

The transport barrier isolates chaotic orbits in two areas. Therefore, whenever a shearless barrier disappears the chaotic orbits merge together leading to global transport. We conclude that the shearless curves break up and reappear, takes place by local changes of the rotation number profile due to variations of safety factor profile.

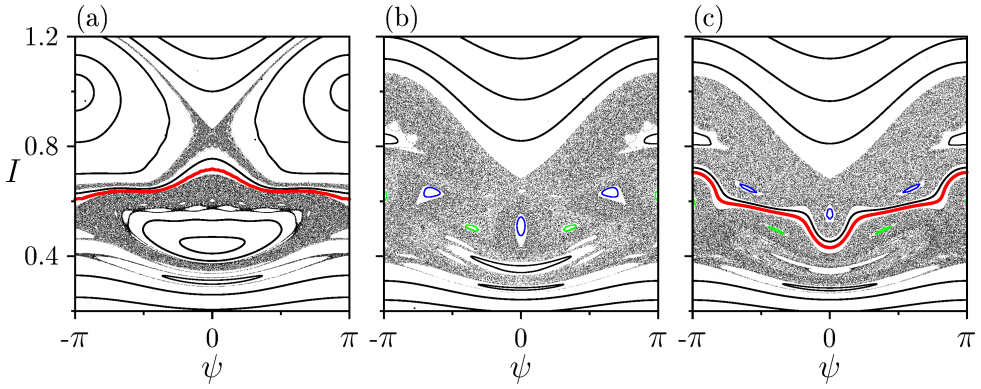

Figure 2: Poincaré sections for given values of safety factor: (a) $q_a = 4.20$, (b) $q_a = 3.44$ and (c) $q_a = 3.40$. The shearless curve (red line) is broken for some intervals of q_a, as seen in (b).

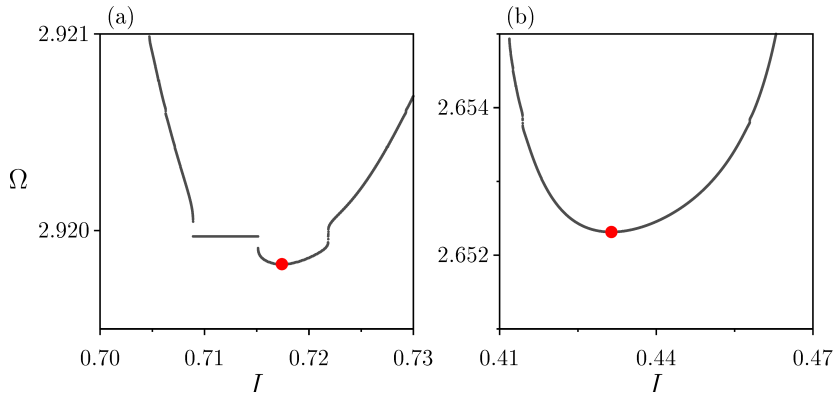

Figure 3: Rotation number profile corresponding to the Poincaré sections depicted in Figures 2(a) and (e). The extrema for each case are marked by red points and indicate a shearless curve.

Acknowledgments: The authors thank the financial support from the Brazilian Federal Agencies (CNPq) under Grant Nos. 407299/2018-1, 302665/2017-0, 403120/2021-7, and 301019/2019-3; the São Paulo Research Foundation (FAPESP, Brazil) under Grant Nos. 2018/03211-6 and 2022/04251-7; and support from Coordenação de Aperfeiçoamento de Pessoal de Nível Superior (CAPES) under Grants No. 88887.522886/2020-00, 88881.143103/2017-01 and Comité Français d'Evaluation de la Coopération Universitaire et Scientifique avec le Brésil (COFECUB) under Grant No. 40273QA-Ph908/18.

References

[1] W. Horton, S. Benkadda, ITER Physics (World Scientific, 2015).

[2] W. Horton, Turbulent transport in magnetized plasmas, 2nd ed. (World Scientific, 2018).

[3] E. Joffrin, et al., Plasma Phys. Control. Fusion **44**, 1739 (2002).

[4] R. C. Wolf, Plasma Phys. Control. Fusion **45**, R1 (2002).

[5] I. L. Caldas, et al., Plasma Phys. Control. Fusion **54**, 124035 (2012).

[6] W. Horton, et al., Physics of Plasmas **5**, 3910 (1998).

[7] P. J. Morrison, Physics of Plasmas **7**, 2279 (2000).

[8] F. A. Marcus, et al., Physics of Plasmas **15**, 112304 (2008).